 BNL 38508

LATE STAGES OF MASSIVE STAR EVOLUTION AND NUCLEOSYNTHESIS

BNL--38508

DE87 001367

Ken'ichi Nomoto and Masa-aki Hashimoto

Department of Physics, Brookhaven National Laboratory
Upton, NY 11973, U.S.A.

on leave from the Department of Earth Science and Astronomy
College of Arts and Sciences, University of Tokyo
Meguro-ku, Tokyo 153, Japan

A lecture delivered at International School of Nuclear Physics, 10th Course
The Early Universe and Its Evolution
Erice, April 2 - 14, 1986

to be published in *Progress in Particle and Nuclear Physics*, Vol 18, 1986

LATE STAGES OF MASSIVE STAR EVOLUTION AND NUCLEOSYNTHESIS

Ken'ichi Nomoto and Masa-aki Hashimoto

Department of Physics, Brookhaven National Laboratory
Upton, NY 11973, U.S.A.

on leave from the Department of Earth Science and Astronomy
College of Arts and Sciences, University of Tokyo
Meguro-ku, Tokyo 153, Japan

ABSTRACT

The evolution of massive stars in the mass range of 8 - 25 $M_\odot$ is reviewed. The effect of electron degeneracy on the gravothermal nature of stars is discussed. Depending on the stellar mass, the stars form three types of cores, namely, non-degenerate, semi-degenerate, and strongly degenerate cores. The evolution for these cases is quite distinct from each other and leads to the three different types of final fate. It is suggested that our helium star model, which is equivalent to a 25 $M_\odot$ star, will form a relatively small mass iron core despite the faster $^{12}C\ (\alpha,\gamma)\ ^{16}O$ reaction.

KEYWORDS

Stellar evolution; gravothermodynamics; nucleosynthesis; supernovae.

I. INTRODUCTION

Big Bang nucleosynthesis produces helium and some other light elements but not beyond, because ^8Be is unstable and the expansion of the universe is too fast and its density is too low to synthesize ^{12}C through the 3α reaction (e.g., Schramm 1986 for a recent review). In other words, the decrease in temperature is much faster than nuclear reactions that tend to realize nuclear statistical equilibrium (NSE) for the corresponding temperature.

However, the universe provides another site of nucleosynthesis. As a result of decreasing temperature, gravitational forces become effective and form stars (before or after the galaxy formation). Stars then evolve. Their internal temperature increases, not decreases, and eventually reaches the ignition temperature of nuclear burning. Starting from hydrogen burning, helium, carbon, oxygen, neon, and silicon burn successively and synthesize heavier elements as the interior temperature continues to increase. This process is considered to be approaching NSE and eventually iron peak elements are synthesized. Finally those elements are ejected from stars into space by means of stellar wind and a supernova explosion. This is the origin of heavy elements.

In constructing the theory of element synthesis, the key is to understand why and how stars evolve, or why stars increase their interior temperature and density and develop a complex structure. Therefore we start from the thermodynamics of self-gravitating system, i.e, gravothermodynamics (Sugimoto et al. 1981), which is described in the next section. The actual evolution of non-degenerate massive stars ($M \sim 25$ $M_\odot$), 10 - 13 $M_\odot$ stars which develop semi-degenerate cores, and 8 - 10 $M_\odot$ stars which form strongly electron degenerate cores, are discussed in §4 - §6, respectively.

II. GRAVOTHERMODYNAMICS AND EVOLUTION OF STARS

Let us consider a system that is governed by its own self-gravity and is in hydrostatic equilibrium. Such a system will eventually undergo the so-called *gravothermal catastrophe* if the density contrast ρ_c/ρ_1 between the center and the outer edge of the system is larger than a certain critical value (see Sugimoto et al. 1981 and references therein). For example, if $\rho_c/\rho_1 > 709$, an isothermal sphere surrounded by an adiabatic wall is secularly unstabe in the following way (Antonov 1960; Lynden-Bell and Wood 1968): If heat is transported from the center to the outer layers, the central region contracts to maintain the hydrostatic equilibrium. Then the central temperature, T_c, increases because gravitational energy release dominates the loss of heat. The resulting temperature gradient promotes more heat flow from the center that induces further gravitational contraction and increase in T_c. The system is said to have a *negative specific heat* because heat loss causes a temperature increase. In other words, the system cannot stay in thermal equilibrium but will move out of equilibrium with increasing T_c/T_1 and ρ_c/ρ_1.

Such a mechanism to create a contrast of density and temperature is easily understood from the behavior of stars which undergo quasi-static gravitational contraction. The hydrostatic stellar structure gives a relation between P_c, ρ_c, and stellar mass, M, as

$$\frac{P_c^3}{\rho_c^4} = 4\pi G^3 \left(\frac{M}{\phi}\right)^2. \tag{1}$$

Here ϕ is the non-dimensional mass and $\phi = 10.73$ and 16.14 for the polytrope of index $\gamma = 1.5$ and 3.0, respectively (Sugimoto and Nomoto 1980; also Arnett 1978). For an ideal gas, Eq.(1) gives

$$\frac{T_c^3}{\rho_c} \sim M^2. \tag{2}$$

The specific entropy, s, is given as

$$\left(\frac{\mu H}{k}\right) s_c = \ln\left(\frac{T_c^{3/2}}{\rho_c}\right) + C_1 = \ln\left(\frac{M^2}{T_c^{3/2}}\right) + C_2 = \ln\left(\frac{M}{\rho_c^{1/2}}\right) + C_3, \tag{3}$$

where μ is the mean molecular weight, H atomic mass unit, k Boltsmann constant, and C_1, C_2, and C_3 additional constants. Equations (2) and (3) show that for the same T_c (i.e, roughly for the same nuclear burning stage), s_c is higher (and ρ_c is lower) for larger M. We need higher entropy to sustain a larger mass against self-gravity.

Another important feature of the stars is that they are open system losing energy by radiation and neutrinos. When nuclear reactions are not active, the star loses entropy, i.e., s_c decreases. From Eq.(3), we see that both T_c and ρ_c increase as s_c decreases for fixed M. In other words, the specific heat in the central region is negative

$$c_g \equiv \frac{ds_c}{d\ln T_c} = -\frac{3}{2}\frac{k}{\mu H}. \tag{4}$$

The increase in ρ_c implies that the star contracts and releases gravitational energy, a part of which goes into internal energy and the rest goes into radiation and neutrino losses. This is the reason why the interior temperature increases during stellar evolution.

As the temperature increases, it reaches the ignition temperature of nuclear burning. Then the star stays in an almost steady state between nuclear energy generation and radiative and neutrino energy losses. When the nuclear fuel is exhausted, the ashes forms a core and nuclear shell burning becomes active around the core. The core undergoes gravitational contraction to increase ρ_c and T_c. On the other hand, the burning shell (denoted by the subscript 1) does not follow the core contraction because, to provide the stellar luminosity, the temperature at the burning shell is almost constant and thus the radius there does not appreciably change. As a result, ρ_c/ρ_1 becomes so large that the core edge can be regarded as a stellar surface. Then the relation expressed by Eq.(1) is applied to the core by replacing M by the core mass M_1. The core can be regarded as a *single star* (Hayashi et al. 1972). (The above role of the active burning shell is crucial when stars evolve to red-giants. See Sugimoto and Nomoto 1980 for more detail.) The smaller M_1 than M is consistent with smaller s_c than that for a previous stage. Further decrease in s_c again leads to increase in T_c until the ash is ignited. The cycle of gravitational contraction and nuclear burning leads to the formation of an onion-like chemical structure as will be shown in later sections.

In short, the star evolves because it is a self-gravitating system and has a *negative specific heat*. The sign of the *specific heat* depends on the equation of state, however. If the entopy is sufficiently high, the pressure depends on temperature. The decrease in entropy results in decrease in temperature and thus pressure, if density is fixed. Then, to maintain hydrostatic equilibrium, the star has to contract to increase the density and temperature. This situation is completely opposite if electrons are degenerate and the pressure does not much depend on temperature. In this case, the loss of entropy does not much affect the hydrostatic equilibrium and thus does not induce gravitational contraction. Accordingly T_c decreases as the star loses energy. In other words, the star has a *positive* specific heat and eventually becomes a cold white dwarf. By applying the equation of state for non-relativistic degenerate electrons, $P = K_1\rho^{5/3}$, to Eq.(1), we obtain a relation,

$$\rho_c \sim M^2. \tag{5}$$

If electrons are relativistically degenerate, i.e., $P = K_2\rho^{4/3}$, Eq.(1) gives the Chandrasekhar mass. Such a change in equation of state occurs for stars with sufficiently low central entopy and thus for a sufficiently small mass, M, or small core mass, M_1, as seen from Eq.(3). Of cource, M or M_1 should be smaller than the Chandrasekhar mass.

The example of the evolutionary change in the central density and temperature during the gravitational contraction is shown in Figures 1 and 2 for neon stars with masses 1.30 - 1.45 $M_\odot$ (Nomoto 1984a, 1986). These evolutionary paths follow the relation given in Eq.(1) for fixed M. At the peak temperature, the gravothermal specific heat changes its sign because electrons become strongly degenerate. The peak temperature is higher for larger M as seen in Figure 3 (Nomoto 1984a) because larger masses correspond to higher T_c for the same ρ_c in the non-degenerate regime (Eq. 2) and higher central densities for the degenerate regime (Eq. 5). If M is so small that the peak temperature is lower than the ignition temperature of the nuclear fuel, the star will become a white dwarf. On the other hand, if M is large enough, T_c can reach the ignition temperature. Therefore, there exists a minimum mass for nuclear burning to occur. The minimum mass is 0.08, 0.25, 1.06, and 1.37 $M_\odot$ for hydrogen, helium, carbon, and neon burning, respectively (e.g., Arnett 1978; Nomoto 1981 for a review).

Therefore, stars with a core mass, M_1, smaller than the above minimum mass will not undergo further nuclear burning, but form a white dwarf-like degenerate core. In this sense, the stellar mass, M, is a critical parameter to determine the final fate of evolution and the stellar evolution is classified by M as follows:

1) For $M < 0.08\ M_\odot$, the star will become a planet-like black dwarf without igniting hydrogen burning.

2) For $0.08\ M_\odot < M < 0.45\ M_\odot$, the star will end up as a helium white dwarf, though such a single star is still a red-dwarf on the main-sequence because hydrogen cannot be depleted within a Hubble time.

3) For $0.45\ M_\odot < M < 8\ M_\odot$, the star forms a degenerate C+O core. Most of them will become a C+O white dwarf by losing their hydrogen-rich envelope, but some of them (~ 6 - $8\ M_\odot$) could reach a supernova stage by increasing the C+O core mass to the Chandrasekhar mass and ignites a carbon deflagration. The mechanism is the same as of Type Ia supernovae but, because of the existence of a hydrogen-rich envelope, the explosion will look like a Type II-L supernova (Doggett and Branch 1985).

4) For 8 - 10 $M_\odot$ range, a degenerate O+Ne+Mg core is formed. The star will eventually collapse due to electron capture on ^{24}Mg and ^{20}Ne.

5) For 10 - 13 $M_\odot$ range, neon is ignited in a semi-degenerate O+Ne+Mg core. Whether subsequent evolution leads to a non-degenerate or a degenerate configuration depends on neutronization during oxygen burning.

6) For $M > 13\ M_\odot$, the star undergo non-degenerate burning to form an iron core.

Typical evolution for cases 4) - 6) will be discussed in §4 - §6, respectively. (See Iben 1986 for smaller mass stars.)

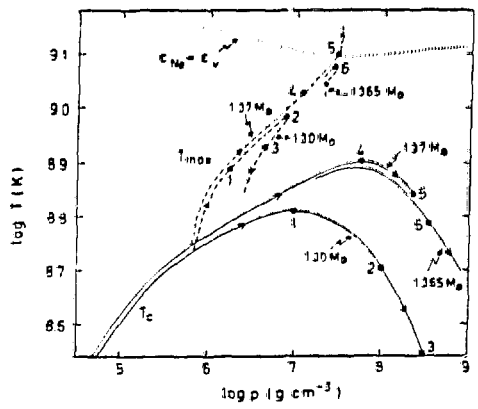

Fig. 1

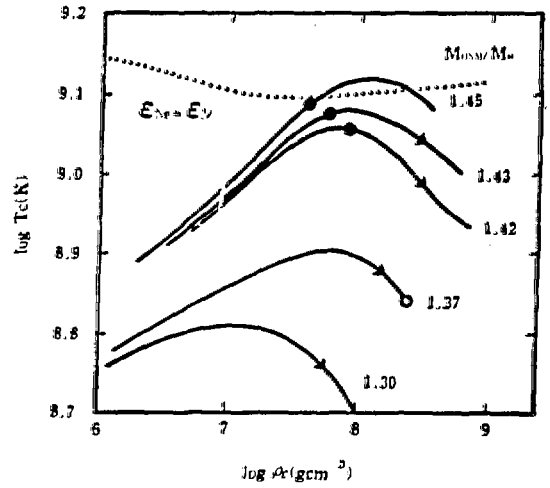

Fig. 2

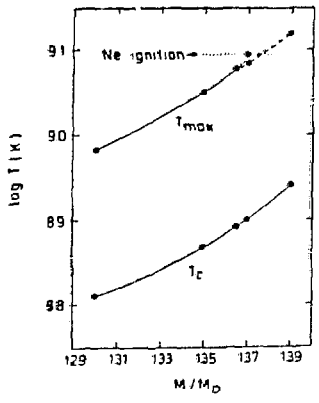

Fig. 3

Figure 1: Evolutionary change in the central density and temperature of neon stars during gravitational contraction (Nomoto 1984a).

Figure 2: Same as Figure 1 but for neon stars of larger mass (Nomoto 1986).

Figure 3: The peak values of T_c and T_{max} given in Figure 1 as a function of neon star mass, M. The dotted line indicates the neon ignition line (Nomoto 1984a).

III. MODELS

The present set of evolutionary calculations has been performed by Hashimoto and Nomoto (1986) for helium stars of mass M_α = 2.8 $M_\odot$, 3.0 $M_\odot$, 3.3 $M_\odot$, 6 $M_\odot$, and 8 $M_\odot$. These helium star masses correspond to the main-sequence mass of $M_{ms} \simeq$ 11, 12, 13, 19, and 25 $M_\odot$, respectively. The calculations started from the gravitational contraction of the helium star. The input physics is mostly the same as used in Nomoto (1984a) and Nomoto et al. (1984). The nuclear reaction network has been developed by Hashimoto et al. (1983) and the reaction rates are based on Fowler et al. (1975), Harris et al. (1982), Caughlan et al. (1985), Woosley et al. (1975, 1978), and Thielemann (1986). The initial composition is assumed to be $X(^4\mathrm{He}) = 0.9879$ and $X(^{14}\mathrm{N}) = 0.0121$. The heavier elements are taken into account in the opacity. The weak rates are taken from Fuller et al. (1980, 1982).

In Figure 4, evolution of the central density, ρ_c, and temperature, T_c, is shown for these cases. The approximate ignition lines for carbon, neon, oxygen, and silicon, where the nuclear energy generation rate is equal to neutrino energy losses, are shown. The line for ψ = 10 approximately divides the electron degenerate and non-degenerate region, where ψ is the chemical potential of an electron in units of kT. The helium stars of M_α = 8 and 6 $M_\odot$ clearly undergo nuclear burning under non-degenerate conditions. For comparison, the evolutionary path of the 2.2 $M_\odot$ helium core is shown, which enters the strongly degenerate region after carbon burning. For M_α = 2.8 - 3.3 $M_\odot$, the O+Ne+Mg core becomes semi-degenerate and whether they will enter degenerate or non-degenerate region is an interesting question. The evolution has been calculated up to the exhaustion of oxygen. The most important improvement from the previous calculations is that we include a more extensive nuclear reaction network and found that even before the oxygen exhaustion, the decrease in electron mole numb[illegible], Y_e, is significant (see also Arnett and Thielemann 1985; Thielemann and Arnett 1985). The implication of these results is discussed for each case in §4 - §6.

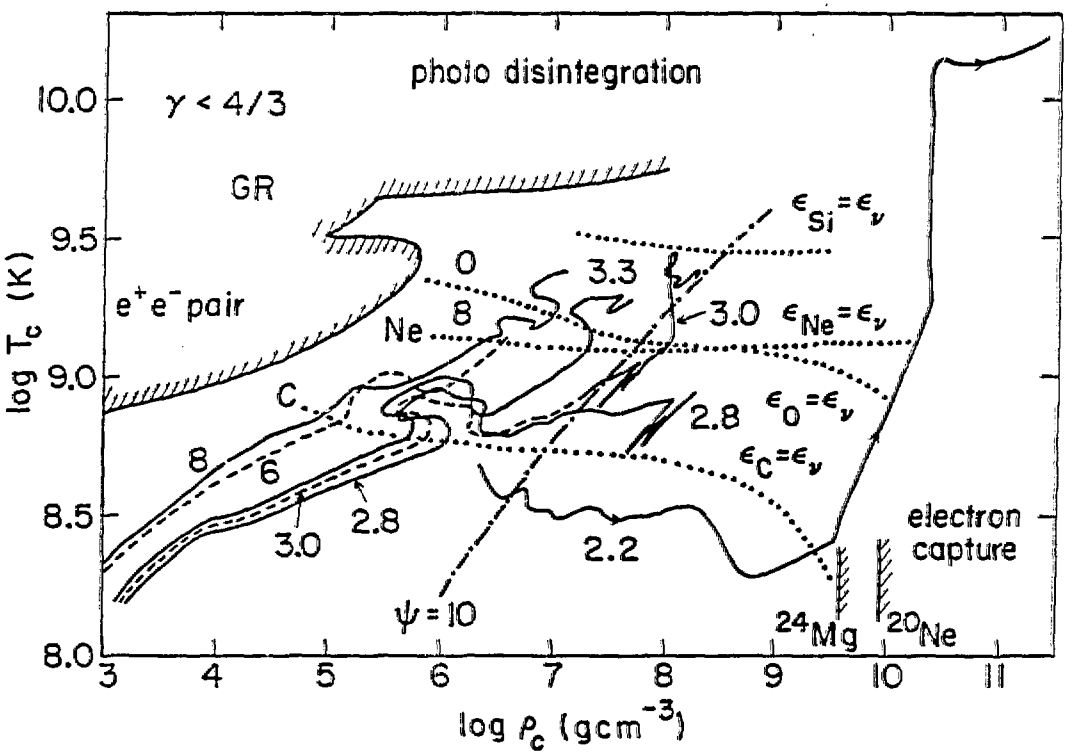

Figure 4: Evolution of the central density, ρ_c, and temperature, T_c for helium stars of mass M_α = 8, 6, 3.3, 3.0, 2.8, and 2.2 $M_\odot$.

IV. EVOLUTION OF MASSIVE STARS ($M \sim 25\ M_\odot$)

Stars with main-sequence mass of $M_{ms} \simeq 20$ - $25\ M_\odot$ have been considered to be one of the most important sites of nucleosynthesis because they produce most species from oxygen to iron peak elements with reasonable accord to the solar abundance ratios (e.g., Woosley and Weaver 1986b). It is also possible to compare the theoretcal prediction of nucleosynthesis with the *observed* abundance of supernova ejecta which is obtained from supernova spectra and supernova remnants. Therefore it is important to calculate the detailed nucleosynthesis history of stars in this mass range.

Recent revision of $^{12}C\ (\alpha,\gamma)\ ^{16}O$ rate has substantially changed the evolution of massive stars (e.g., Fowler 1984). Due to the ~ 3 times larger $^{12}C\ (\alpha,\gamma)\ ^{16}O$ rate, the abundance of carbon produced by helium burning is significantly smaller than the previous value (Woosley and Weaver 1986a,b). This affects not only the nucleosynthesis yield, but also stellar structure and thus the final iron core mass. In the $25\ M_\odot$ model by Woosley and Weaver (1986a), the iron core is as massive as $2.1\ M_\odot$. The transition from the iron core mass from $1.35\ M_\odot$ to $2\ M_\odot$ occurs around $M_{ms} \sim 18\ M_\odot$. Such a large iron core mass has given a big impact on supernova modeling because the prompt shock mechanism does not work for such a core (e.g., Kahana 1986; Hillebrandt 1986).

However, the carbon abundance is subject to uncertainties. It depends not only on $^{12}C\ (\alpha,\gamma)\ ^{16}O$ rate, but also on how the convective core grows, and thus, on the treatment of the convective core edge and overshooting. In particular, if the convection core grows substantially near the end of helium burning, fresh helium is mixed into the high temperature region and processes ^{12}C into ^{16}O very efficiently. Since no reliable theory of convection, especially non-local theory, exists at the moment, it is necessary to explore the various possible evolutionary paths within a uncertain range. As a first step, we report our preliminary calculations for the helium star of $M_\alpha = 8\ M_\odot$ which is almost equivalent to $M_{ms} = 25\ M_\odot$. We adopt the Schwarzshild criterion for convective stability and neglect the overshooting (e.g., Langer 1986).

4.1 Stellar Structure

First let us look at some evolutionary features of this star from the density distribution in Figure 10. The stage numbers refer to 1: helium burning, 2: exhaustion of helium, 3: carbon ignition, 4: neon ignition, 5: oxygen ignition, and 6: exhaustion of oxygen. The evolutionary change in the density distribution depends on the timescale of entropy loss from the central region, which is mainly determined by the neutrino luminosity, L_ν. During the quasi-static contraction, the decrease in entropy due to neutrino losses promotes the contraction as seen from Eq.(3). For nuclear burning stages, nuclear luminosity, L_n, is balanced with L_ν so that the entropy in the convective layer is almost stationary. However, the depletion timescale of nuclear fuel is determined by L_n and thus related to L_ν. As T_c increases, L_ν increases rapidly, which accelerates the evolution. As seen from Figure 10, the whole helium star contracts up to stage 2. Later, the density structure in the outer layers is practically frozen since the timescale of energy transport from the central region to the outer layers is much longer than the evolutionary timescale near the center. In this sense, the *effective core mass*, M_{core}, which replaces M in Eq.(1)-(3), is decreasing. When shell burning is active, its location, M_r, gives the approximate value of M_{core} as discussed in §2.

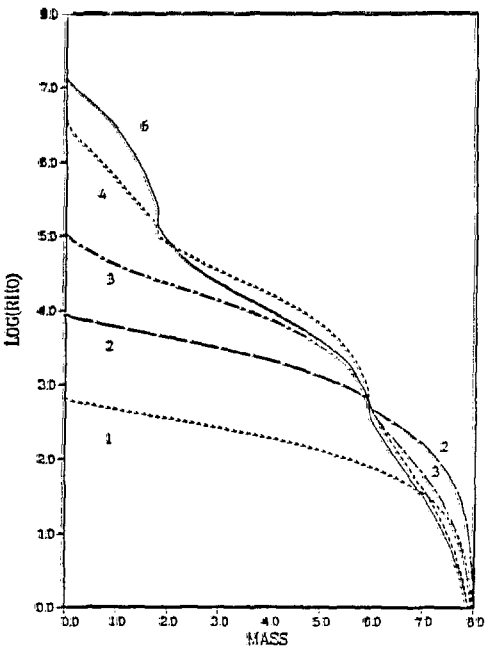

Figure 5: The evolutionary change in the density distribution for a helium star of $M_\alpha = 8\ M_\odot$.

4.2 Helium, Carbon, and Neon Burning and Carbon Abundance

The helium burning stage lasts for 7.35×10^5 yr and a C+O core of 6.0 $M_\odot$ forms. The mass fractions of carbon and oxygen are $X(^{12}C) = 0.19$ and $X(^{16}O) = 0.79$, respectively, as seen in Figure 6. This amount of carbon is small due to the faster $^{12}C\ (\alpha,\gamma)\ ^{16}O$ reaction, but still sufficiently large that the carbon burning rate exceeds the neutrino energy losses when $T_c = 8.0 \times 10^8$ K. Carbon burning starts in the center (stage 3: 8.4×10^3 yr after exhaustion of helium) and forms a convective core of 0.27 $M_\odot$. The compostion structure at carbon ignition is shown in Figure 6. The carbon burning phase lasts only 100 yr. When carbon is almost depleted in the core, the resultant composition is $X(^{16}O) = 0.70$ and $X(^{20}Ne) = 0.25$. Because of the small carbon abundance, the O/Ne ratio is large compared with the model based on the old low $^{12}C\ (\alpha,\gamma)\ ^{16}O$ rate (Weaver et al. 1978). The carbon burning layer shifts to the outer shell and a convective shell develops at $M_r = 0.94$ - 1.78 $M_\odot$. When neon is ignited in the center (stage 4: 40 yr after exhaustion of carbon), only a trace of carbon is left interior to $M_r < 1.78\ M_\odot$, and a convective carbon burning shell forms at $M_r = 1.79$ - 5.4 $M_\odot$. Neon burning lasts for 0.4 yr and forms a convective core of 0.42 $M_\odot$. After exhaustion of neon in the center, an oxygen-rich core of $X(^{16}O) = 0.82$ and $X(^{24}Mg) = 0.08$ forms (Figure 8) and a convective neon burning shell appears at $M_r = 0.42$ - 0.90 $M_\odot$.

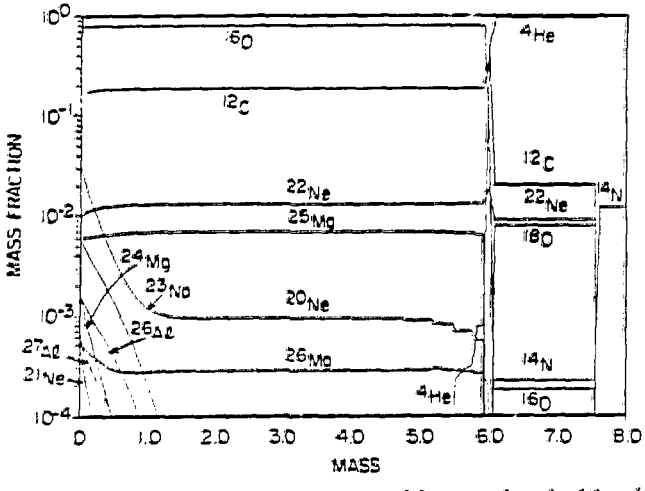

Figure 6: Composition of a helium star of $M_\alpha = 8\ M_\odot$ at carbon ignition (stage 3).

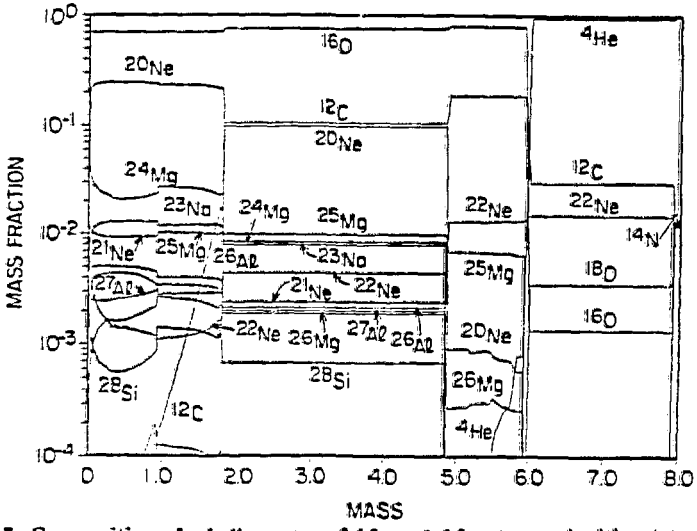

Figure 7: Composition of a helium star of $M_\alpha = 8\ M_\odot$ at neon ignition (stage 4).

4.3 Oxygen Burning Stage

At stage 5, oxygen is ignited in the center (Figure 8). A convective core extends to $M_r = 0.99\ M_\odot$. Oxygen burning synthesizes silicon and sulfur - rich elements. As oxygen burning proceeds, the product is getting neutron-rich. The main weak processes involved are: 1) positron decays, $^{31}S\ (\beta^+)\ ^{31}P$, $^{30}P\ (\beta^+)\ ^{30}Si$, and $^{34}Cl\ (\beta^+)\ ^{34}S$ and 2) electron captures, $^{33}S\ (e^-, \nu)\ ^{33}P$ and $^{35}Cl\ (e^-, \nu)\ ^{35}S$. When $X(^{16}O) \simeq 0.013$, Y_e drops to 0.493 (neutron excess $\eta \equiv 1 - 2Y_e = 0.014$) in the convective core where ^{28}Si , ^{32}S , and ^{38}Ar are the main constituents (Figure 9). At this stage, a convective shell of neon burning starts to form at $M_r = 1.00\ M_\odot$.

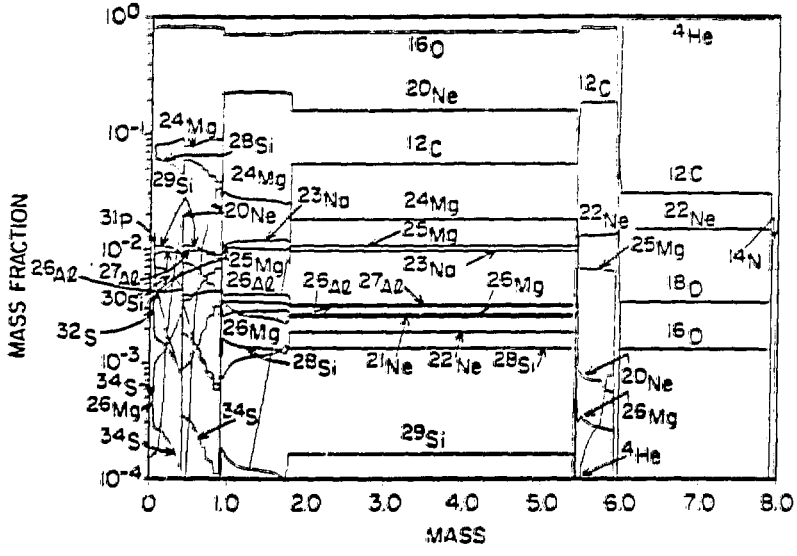

Figure 8: Composition of a helium star of $M_\alpha = 8\ M_\odot$ at oxygen ignition (stage 5).

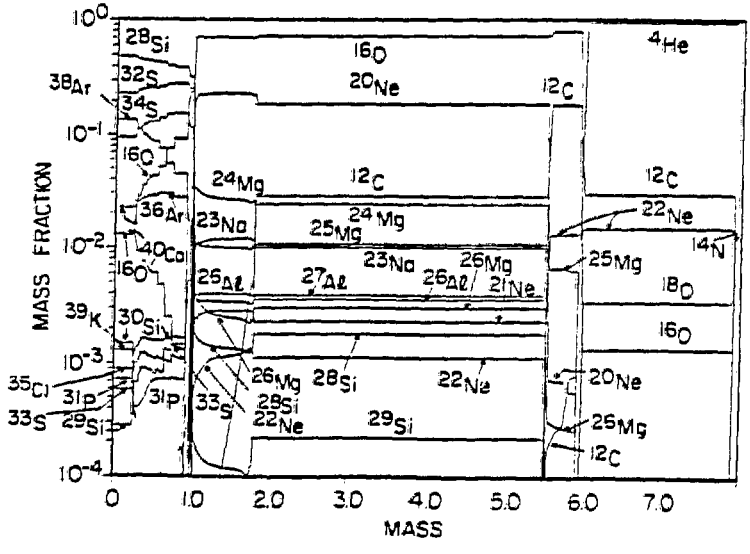

Figure 9: Composition of a helium star of $M_\alpha = 8\ M_\odot$ near the end of oxygen burning where $X(^{16}O) \simeq 0.013$ (stage 6).

4.4 Comparison with the Previous Models

Our result is similar to the 25 $M_\odot$ model of Woosley and Weaver (1986a; WW25 model) in the sense that the faster ^{12}C (α,γ) ^{16}O reaction reduces the abundances of carbon, neon, and magnesium, while it increases the oxygen abundance. On the other hand, there are some differences. In the WW25 model, no convective core appears for carbon and neon burning phases, while, in our model, both carbon and neon burning dominate the neutrino energy losses and thus, a small convective core and then an extensive convective shell form. In particular, convective carbon burning shell extending from $M_r = 1.79$ $M_\odot$ to 5.4 $M_\odot$ is quite active during neon and oxygen burning. As a result, a sharp entropy increase appears at $M_r = 1.8$ $M_\odot$ ($s = 5.0$ k/H in the carbon burning shell). The existence of active burning shell makes the *effective core mass* in Eq.(1) smaller, which correspondis to the smaller central entropy. In fact, at oxygen ignition, s_c is as low as 1.9 k/H ($\psi_c \simeq 2.8$) which is almost equal to that of the 15 $M_\odot$ WW model and smaller than that of the WW25 model by a factor of 1.5. The entropy distribution in our model is very similar to the old 25 $M_\odot$ model by Weaver, Woosley, and Fuller (1985, WWF). This is because our carbon abundance is about twice that of the WW model, which may be due to differences in the treatment of convection. Since the WWF 25 $M_\odot$ model forms a 1.35 $M_\odot$ iron core, our model is expected to form such a small iron core.

During oxygen burning, positron emissions and electron captures increase η. Though $\eta \simeq 0.014$ at $X(^{16}O) \simeq 0.013$ in this model, η is larger in smaller mass stars and has important effects on the later evolution and nucleosynthesis (§5). Nucleosynthesis in our model is consistent with more detailed network calculation based on the polytropic models by Thielemann and Arnett (1985).

V. EVOLUTION OF 10 - 13 $M_\odot$ STARS

The evolution of stars in the mass range of $M_{ms} = 10$ - 13 $M_\odot$ ($M_\alpha \simeq 2.5$ - 3.3 $M_\odot$) is significantly different from 25 $M_\odot$ stars, being more complicated and sensitive to the stellar mass. This is because electrons become somewhat degenerate, which affects the structure of the core. Stars in this mass range undergo non-degenerate carbon burning and form an oxygen-neon core whose mass, M_{ONe}, is in the range of 1.37 - 1.5 $M_\odot$. The core mass M_{ONe} is large enough to ignite neon, yet the core is semi-degenerate and the degree of degeneracy depends sensitively on how close M_{ONe} is to the Chandrasekhar mass.

5.1 Nucleosynthesis during Helium and Carbon Burning

The evolution during helium and carbon burning is qualitatively similar to the 25 $M_\odot$ star but quantitatively different due to the smaller mass and thus lower central temperature during nuclear burning. As an example of this mass range, Figures 10 - 12 show the chemical composition of the helium star of $M_\alpha = 2.8$ $M_\odot$ ($M_{ms} \simeq 11$ $M_\odot$). Helium burning forms a C+O core of 1.23 $M_\odot$. The abundances are $X(^{12}C) = 0.29$ and $X(^{16}O) = 0.69$ (Figure 10). The mass fraction of carbon is 0.28 - 0.29 for this mass range, which is larger than in the 25 $M_\odot$ model due to the lower central temperature. The old ^{12}C (α,γ) ^{16}O rate gives $X(^{12}C) \simeq 0.5$ for $M_{ms} \sim 10$ $M_\odot$ (e.g., Arnett 1972). The helium burning shell advances gradually in mass and thus the C+O core mass grows as $M_{CO} = 1.345$, 1.415, and 1.423 $M_\odot$ at the stage of carbon ignition, exhaustion of carbon, and neon ignition, respectively. Note that M_{CO} is less than the Chandrasekhar mass but larger than the critical mass of 1.37 $M_\odot$ for neon ignition.

Carbon burning ignites in the center and forms an oxygen-neon core of about 0.6 $M_\odot$. The oxygen-neon core contains more oxygen than neon and their mass fractions are $X(^{16}O) = 0.56$, $X(^{20}Ne) = 0.33$, and $X(^{24}Mg) = 0.06$ (Figure 11). The oxygen/neon ratio is almost the reverse of that in the old models because of the small carbon abundance in the present model. The ^{24}Mg abundance is also small for the same reason.

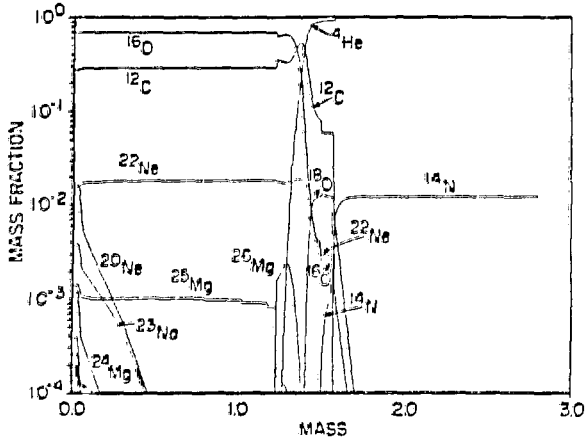

Figure 10: Abundances in the 2.8 $M_\odot$ helium star at carbon ignition in the center (stage 2).

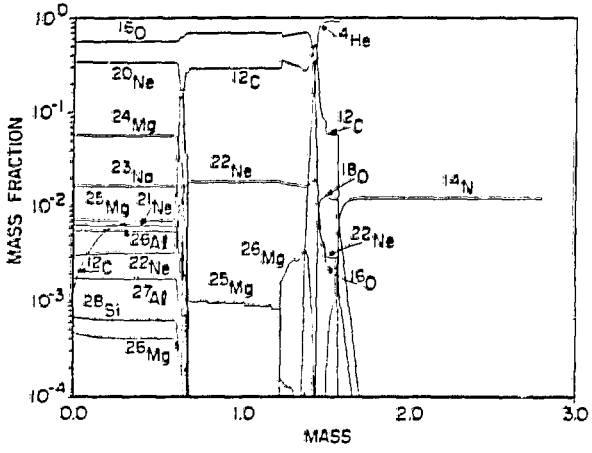

Figure 11: Same as Figure 10 but at exhausion of carbon (stage 3).

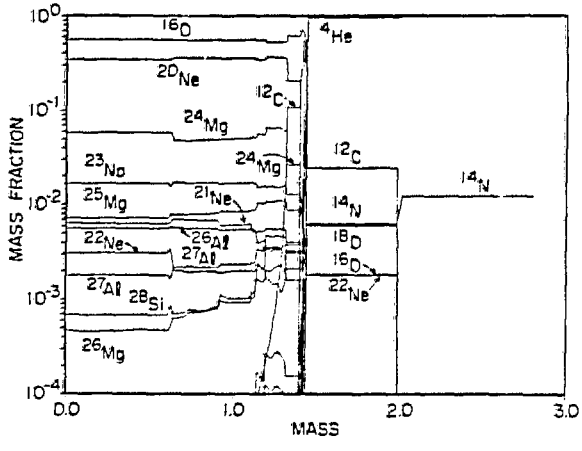

Figure 12: Same as Figure 10 but at neon ignition (stage 6).

5.2 Semi-Degenerate Oxygen-Neon Core and Off-Center Neon Ignition.

The oxygen-neon core grows and contracts as the carbon burning shell advances. The evolution of (ρ_c, T_c) in Figure 3 is determined by the increasing oxygen-neon core mass, M_{ONe}, as given in Eq.(1). Since the core is somewhat degenerate, compressional heating is slower than the neutrino cooling. Therefore, the central temperature does not increase while ρ_c increases. The electrons become degenerate in the central region, i.e., the (ρ_c, T_c) path enters the region of $\psi > 10$. When M_{ONe} reaches the critical mass of 1.37 $M_\odot$, neon burning ignites not in the center, but in the outer shell. The location of the neon ignition depends on the degree of electron degeneracy and thus on the stellar mass.

The formation of a semi-degenerate core gives several distinct features to stars of $M_\alpha = 2.5$ - $3.2\ M_\odot$. Let us first look at the overall evolution from the evolutionary change in density and temperature distributions of the helium star of $M_\alpha = 2.8\ M_\odot$ ($M_{ms} \sim 11\ M_\odot$) (Figures 13 and 14). The stage numbers correspond to 1: exhaustion of helium, 2: ignition of carbon burning, 3: exhaustion of carbon, 4-5: development of a temperature inversion in the O-Ne core, 6: off-center ignition of neon, 7-8: propagation of the neon burning layer.

First we note that the star forms a quite remarkable core - envelope structure (Figure 10). As the core contracts, the helium envelope expands. The helium burning shell is a node and a very steep density gradient appears at the helium burning shell ($M_r = 1.42\ M_\odot$). The radius of this helium star reaches 12 $R_\odot$. This is the same phenomena as a star expands from the main-sequence to the giant branch (Sugimoto and Nomoto 1980). For $M_\alpha = 8\ M_\odot$, the core - envelope feature is less pronounced, because the evolutionary timescale after carbon burning is too short for the effect of core contraction to be transmitted to the helium layer.

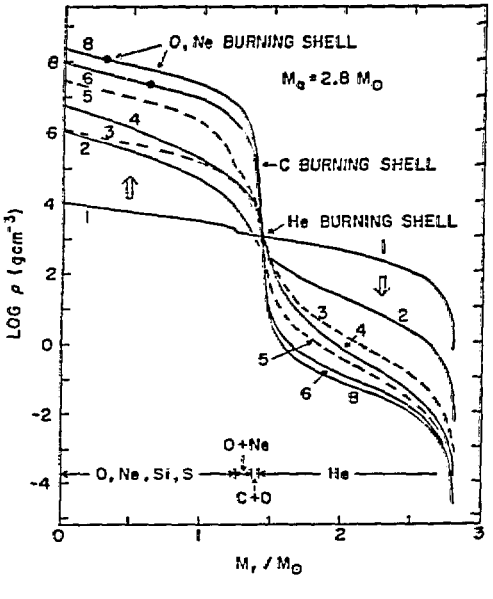

Figure 13 (left): Evolutionary change in the density distribution for $M_\alpha = 2.8\ M_\odot$.

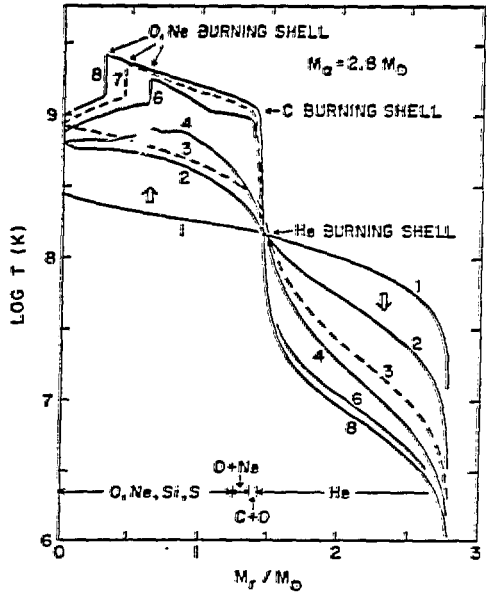

Figure 14 (right): Same as Figure 13 but for temperature.

Secondly, stars in this range develop a temperature inversion in the central region (Figure 11), because neutrino energy losses are faster at higher densities. In such a core, the pressure necessary to sustain hydrostatic equilibrium is provided by degenerate electrons. The temperature inversion leads to an off-center ignition of neon at $M_r = 0.78$, 0.64, 0.30, and 0.10 $M_\odot$ for $M_\alpha = 2.6$, 2.8, 3.0, and 3.2 $M_\odot$, respectively (see, e.g., Nomoto 1984a; Habets 1985, 1986). For $M_\alpha = 3.3$ $M_\odot$, electron degeneracy is so weak that the temperature inversion does not appear and neon ignites at the center. Therefore, the critical main-sequence mass that discriminates beween off-center and central ignition of neon is $M_{ms} \sim 13$ $M_\odot$.

5.3 Propagation of Neon-Oxygen Burning Layer

When neon ignites off-center, shell burning is unstable to a flash due to electron degeneracy. The flash increases the temperature to as high as 2×10^9 K and forms a sharp temperature jump as seen in Figure 14. Subsequently the neon burning shell propagates inward (Figure 14). An important question is whether or not the burning shell reaches the center. If not, a degenerate oxygen-neon core is left unburned as found by Barkat et al. (1974) and also in the Woosley and Weaver's (1986a) 11 $M_\odot$ model. This is crucial in determining the final fate of stars.

Figure 15 shows the propagation of the neon burning layer for $M_\alpha = 3.0$ $M_\odot$. As the burning front moves to the higher density layers, the temperature increases to $2.0 - 2.5 \times 10^9$ K. At such high temperature, oxygen also burns to synthesize silicon and sulfur. The composition profile during the propagation is shown in Figure 16. The burning front propagates all the way to the center. Since the density at the neon burning front does not become so high ($\rho < 10^8$ g cm^{-3}) and also neon ignites layer by layer, the released energy in O-Ne flash is too small to induce major dynamical effects.

For slightly smaller mass of $M_\alpha = 2.8$ $M_\odot$, on the other hand, the neon burning front reaches densities as high as $\rho > 10^8$ g cm^{-3}. Then the neon shell flashes become so explosive that a dynamical event, such as ejection of a helium layer, is expected (also Woosley et al. 1980). Therefore, it is crucial whether the neon burning front can reach high densities or is quenched by neutrino cooling at an earlier stage.

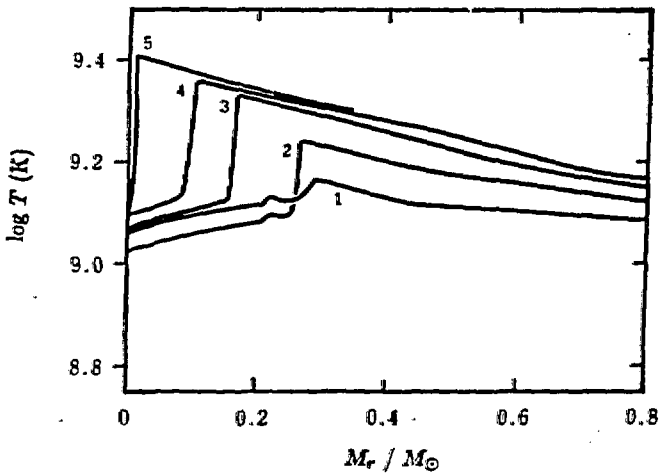

Figure 15: Change in the temperature profile during the propagation of the neon burning front for $M_\alpha = 3.0$ $M_\odot$.

The propagation mode of neon burning front is not heat conduction but compressional heating due to gravitational contraction of the oxygen-neon core. This can be seen from the increase in density after the neon ignition in Figure 13. For $M_\alpha = 3.0\ M_\odot$, it takes only 2 yr for the burning front to propagate to the center. This is much faster than conduction (also Ikeuchi et al. 1972; Woosley et al. 1980). In order to sustain the propagating front, compressional heating should dominate neutrino cooling. In other words, the core mass interior to the helium burning shell should be sufficiently large to keep $\epsilon_g < 0$ until T_c reaches the neon ignition temperature. If the core mass is too small relative to the Chandrasekhar mass, electron degeneracy changes the sign of gravothermal specific heat of the core and then the temperature starts to decrease.

In order to clarify this point, simple oxygen-neon star models have been calculated with neon burning artificially suppressed as already shown in Figure 2. Here the stars of mass M_{ONe} are undergoing gravitational contraction. The result shows that for $1.46\ M_\odot > M_{ONe} > 1.37\ M_\odot$ the neon ignition temperature is reached first in the outer shell at the stage marked by open cicle in Figure 2. Afterwards the central temperature also reaches the neon ignition line for $M_{ONe} > 1.44\ M_\odot$, while T_c starts to decrease without igniting neon for smaller mass stars.

If we apply this criterion to the case of $M_\alpha = 2.8\ M_\odot$, its core mass is only $M_{ONe} = 1.42\ M_\odot$ so that neon burning will be quenched with some unburned oxygen-neon in the central region. However, the above criterion is obtained for $Y_e = 0.5$. In the actual neon - oxygen burning, Y_e is decreasing due primarily to electron capture on ^{33}S and ^{35}Cl. For $M_\alpha = 2.8\ M_\odot$, the density at the burning front is as high as 10^8 g cm^{-3} so that Y_e is as low as 0.48 due to electron captures. Such a small Y_e implies that the core mass exceeds the Chandrasekhar mass that is now $\sim 1.38\ M_\odot$ and thus the gravothermal specific heat of the core remains negative. Therefore, the central temperature continues to increase up to the neon ignition temperature. Then the burning layer will reach the center. The propagation of the oxygen-neon shell burning is self-sustanined because electron captures in the burning layer promotes the contraction. This implies that the density at the burning front will become high enough to induce explosive neon flashes for $M_\alpha \simeq 2.6$ - $2.8\ M_\odot$. It may or may not lead to the ejecton of a helium layer (Woosley et al. 1980). The quenching of neon burning would be the case only for very limited mass range, if it occurs at all. The use of a sufficiently large nuclear reaction network is crucial for the study of this mass range.

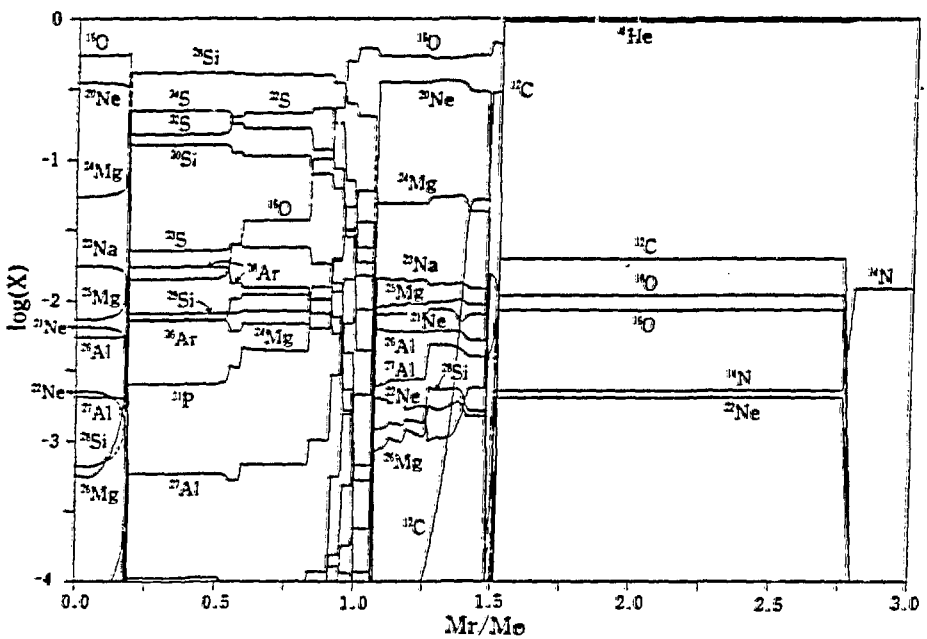

Figure 16: Composition of the helium star of $M_\alpha = 3.0\ M_\odot$ during the propagation of neon and oxygen burning front.

VI. EVOLUTION OF 8 - 10 $M_\odot$ STARS

For this mass range, electron degeneracy becomes significant already in a C+O core. Therefore, several features of the semi-degenerate core discussed in §5 appear earlier, i.e., before carbon ignition. We describe the evolution of a helium *core* of $M_\alpha = 2.2\ M_\odot$ as a typical example for this mass range (Nomoto 1984b). (This is not a helium *star* but a *core* embedded in the hydrogen-rich envelope of a star with $M_{ms} = 8.8\ M_\odot$.) The evolutionary path of (ρ_c, T_c) is seen in Figure 4. Chemical evolution of the core through the end of the dredge-up of a helium layer is shown in Figure 17. Evolutionary changes in the photon luminosity, L_{ph}, L_n, and L_ν are shown in Figure 18. Figure 19 shows changes in ρ_c, T_c, and ψ_c. For the stages where the temperature inversion appears, the maximum temperature within the core, T_{max}, is also plotted. This calculation used the old $^{12}C\ (\alpha,\gamma)\ ^{16}O$ rate so that the details of elemental abundances are not discussed here.

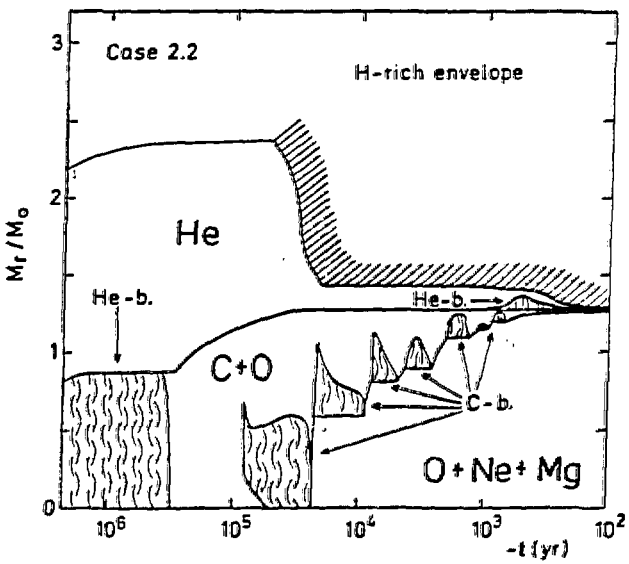

Figure 17: Chemical evolution of the core through the end of the dredge-up of helium layer.

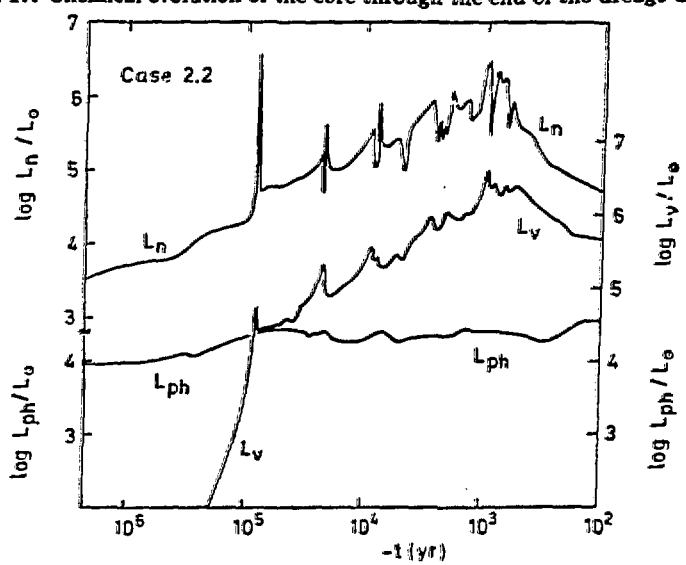

Figure 18: Evolutionary changes in the photon luminosity, L_{ph}, L_n, and L_ν.

6.1 Carbon Burning

In a semi-degenerate C+O core, a temperature inversion appears due to neutrino cooling. This leads to off-center ignition of carbon when the C+O core mass exceeds the critical mass of 1.06 $M_\odot$. (For $M_\alpha >$ 2.6 $M_\odot$, carbon ignites in the center.) The off-center carbon burning shell moves inward all the way to the center as neon shell burning does for $M_\alpha = 2.8 - 3.2\ M_\odot$ (Figure 17). However, the propagation mode is different. For neon burning, it is compressional heating. On the other hand, it is heat conduction for carbon burning. Once ignited, there is no way to prevent the burning front from reaching the center as shown for accreting C+O white dwarfs (Saio and Nomoto 1985; Woosley and Weaver 1986a).

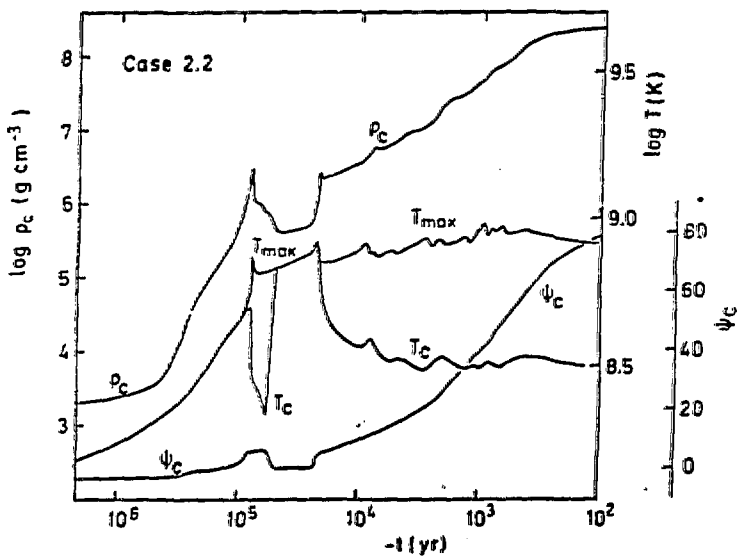

Figure 19: Changes in ρ_c, T_c, and electron chemical potential, ψ_c, in units of kT.

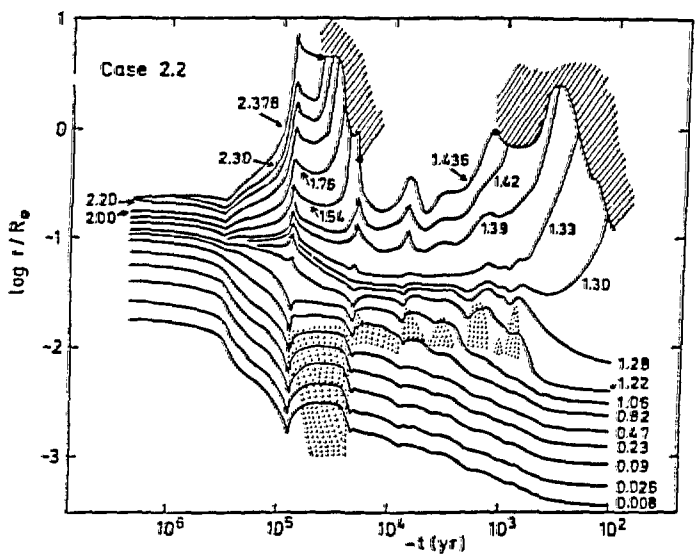

Figure 20: Evolutionary changes in the radial distances from the center for several Lagrangian shells indicated by $M_r/M_\odot$.

6.2 Formation of Strongly Degenerate O-Ne-Mg Core

After exhaustion of carbon in the central region, an O+Ne+Mg core forms. Its mass increases through irregular carbon shell burning. Figure 20 shows evolutionary changes in the radial distances of Lagrangian shells from the center. Here the dotted regions are convective due to carbon burning. It is seen that the carbon burning shell is almost stationary around $r \simeq 0.01\ R_\odot$. The core materials contract, being heated up to the carbon ignition temperature and moving through the burning shell after being converted into oxygen-neon. In this way, ρ_c increases as the mass of the oxygen-neon core increases. At the same time, T_c decreases down to 3×10^8 K due to neutrino emission. It is clear that the specific heat of the core is now positive. This is the important difference from more massive stars. Accordingly, the core becomes strongly degenerate as seen in Figure 4.

Since the advance of the oxygen-neon burning shell stops near the helium burning shell at $M_r = 1.28\ M_\odot$, the oxygen-neon core mass does not exceed the critical mass of 1.37 $M_\odot$ so that neon is never ignited. The maximum temperature attained is 9×10^8 K which is far below the ignition temperature of neon. This is the case for $M_\alpha \simeq 2.0$ - 2.5 $M_\odot$ ($M_{\rm ms} \sim 8$ - 10 $M_\odot$).

If the core mass stays constant ($\sim 1.3\ M_\odot$), the degenerate core will simply cool like a white dwarf. In the core of a red-giant, the core mass grows because hydrogen and helium shell burning processes the material of the hydrogen-rich envelope into carbon -oxygen. (The helium layer has been dredged up by the penetrating surface convection zone when the layer expands by absorbing heat from the core. See Figure 20). In this sense, the core is essentially the same as accreting white dwarfs.

6.3 Collapse of O+Ne+Mg Core induced by Electron Captures

When the core mass grows to 1.38 $M_\odot$, the central density reaches 4×10^9 g cm^{-3}. Degenerate electrons provide another effect on stellar evolution, i.e., the electron Fermi energy exceeds the threshold for electron captures ^{24}Mg (e^-, ν) ^{24}Na (e^-, ν) ^{24}Ne and ^{20}Ne (e^-, ν) ^{20}F (e^-, ν) ^{20}O. The resultant decrease in Y_e triggers collapse (Miyaji et al. 1980; Miyaji and Nomoto 1986).

The hydrodynamical behavior of collapse is somewhat different from the iron core collapse of more massive stars (see, e.g., Hillebrandt et al. 1984; Burrows and Lattimer 1985; Hillebrandt 1986; Baron et al. 1986). The O+Ne+Mg core contains nuclear fuel which ignites during infall. Electron captures occur only in the NSE layer behind the burning front and, therefore, the region of small Y_e is confined to a central region which grows gradually. The collapse is slower than the collapse of the iron core of a massive star until the burning front has propagated to roughly $\sim 0.8\ M_\odot$ (Hillebrandt et al. 1984). Afterwards the collapse accerelates quickly. Y_e in the NSE region of the O+Ne+Mg core is smaller than Y_e in iron cores, because the entropy at the burning front is higher and thus the proton fraction is larger. These two effects result in a homologous core whose mass is smaller and an outer infalling layer which is less dense than is the case in iron core collpase. Such a structure has two effects on the bounce shock. First, the binding energy of the rebounding core is smaller and, hence, the shock wave is initially weaker (Brown et al. 1982; Lattimer et al. 1985). Secondly, the low density in the outer layers makes the shock propagation easier (Hillebrandt et al. 1984). Which effect dominates depends on the details of collapse hydrodynamics.

VII. CONCLUDING REMARKS

We have shown that the evolution and the final fate of stars is determined by their gravothermodynamical nature that depends on the equation of state and thus on the stellar mass. For massive stars, entropy in the interior is high and electrons are non-degenerate. Then the gravothermal specific heat is always negative and the star evolves toward higher density and temperature as the entropy in the center decreases. Eventually nuclear statistical equilibrium is realized through nuclear burning and the iron core forms. On the contrary, smaller mass stars have lower entropy so that electrons become degenerate at a certain stage of evolution. Then c_g turns positive and the interior temperature starts to decrease as the star loses entropy. These two types of evolution lead to two different type of collapse, i.e., the degenerate core contains nuclear fuel while iron core does not. Between these two types, there is a mass range for which the star forms a semi-degenerate core. The evolution is complicated due to off-center neon flashes and thus careful calculation is required to know in which direction (degenerate or non-degenerate) the star evolves.

We note that the entropy structure at oxygen depletion of our 8 $M_\odot$ helium star model, which is equivalent to a 25 $M_\odot$ star, is very similar to the old 25 $M_\odot$ model by Weaer, Woosley, and Fuller (1985, WWF) who used the old $^{12}C\ (\alpha,\gamma)\ ^{16}O$ rate. Since the WWF 25 $M_\odot$ star model forms a 1.35 $M_\odot$ iron core, our model is expected to form a similar small iron core despite our use of faster $^{12}C\ (\alpha,\gamma)\ ^{16}O$ reaction. This is because our carbon abundance after helium burning is about twice that of the latest 25 $M_\odot$ model by Woosley and Weaver (1986a). Such a difference of carbon abundance may be due to differences in the treatment of convection.

We have emphasized the importance of the use of detailed nuclear reaction network before the oxygen exhaustion. If Y_e in the silicon - sulfur layer is significantly small, it affects not only the size of the iron core, but also ^{56}Ni production during supernova explosion. Since the decays of ^{56}Ni and ^{56}Co into ^{56}Fe provide energy for the light curve, the ^{56}Ni mass is the crucial quantity to model the light curve tail of Type II supernovae. It is particularly important for the Wolf-Rayet models of Type Ib supernovae. In the previous models, ^{56}Ni is synthesized when the shock wave passes through silicon-rich layer (Weaver and Woosley 1980; Johnston and Yahil 1984). The density in the oxygen layer is too low to synthesize much ^{56}Ni. If $Y_e < 0.49$, which would be the case for smaller mass stars, the amount of ^{56}Ni would be small as expected from the NSE abundance given as a function of Y_e (Figure 21). Since Y_e is smaller for smaller mass stars (Thielemann and Arnett 1985), we can obtain the lower mass limit of exploding stars that produce sufficiently large amount of ^{56}Ni for their light curves.

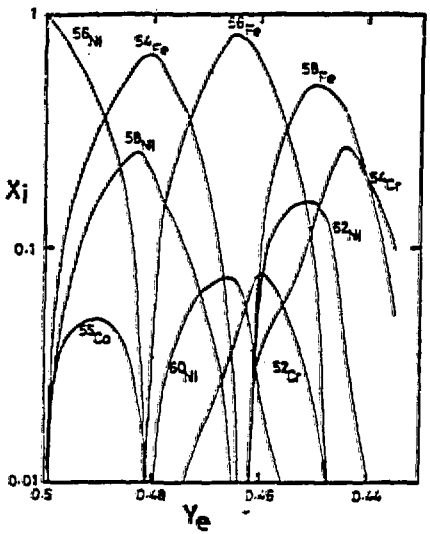

Figure 21: Nuclear statistical equilibrium abundance as a function of electron mole number, Y_e, for $T = 3 \times 10^9$ K and $\rho = 1 \times 10^7$ g cm^{-3}. X_i denotes the mass fraction.

ACKNOWLEDGEMENT

We would like to thank Dr. F.-K. Thielemann for sending us his latest compilation of the nuclear reaction rates and Dr. E. Baron for the reading of the manuscript. It is a pleasure to thank Drs. S.H. Kahana, G.E. Brown, A. Yahil, A. Burrows, and J. Cooperstein for stimulating discussion and hospitality during our stay in Brookhaven and Stony Brook. This work has been supported in part by the U. S. Department of Energy under Contract No. DE-AC02-76CH00016 and by the Japanese Ministry of Education, Science, and Culture through research grant nos. 59380001 and 60540152.

REFERENCES

Antonov, V.A. 1962, *Vest. Leningr. Gos. Univ.*, *7*, 135.
Arnett, W.D. 1972, *Ap. J.*, *176*, 681.
————. 1978, in *Physics and Astrophysics of Neutron Stars and Black Holes*, ed. R. Giaconni and R. Ruffini (Bologna: Soc. Italiana di Fisica), p.356.
Arnett, W.D., and Thielemann, F.-K. 1985, *Ap. J.*, *295*, 589.
Barkat, Z., Reiss, Y., and Rakavy, G. 1974, *Ap. J. (Letters)*, *193*, L21.
Baron, E., Cooperstein, J., and Kahana, S.H. 1986, private communication.
Brown, G.E., Bethe, H.A., and Baym, G. 1982, *Nucl. Phys.*, *A375*, 481.
Burrows, A., and Lattimer, J.M. 1985, *Ap. J. (Letters)*, *299*, L19.
Caughlan, G.R., Fowler, W.A., Harris, M.J., and Zimmerman, B.A. 1985, *Atomic Data and Nuclear Data Tables*, *32*, 197.
Doggett, L.B., and Branch, D. 1985, *A. J.*, *90*, 2303.
Fowler, W.A. 1984, *Rev. Mod. Phys.*, *56*, 149.
Fowler, W.A., Caughlan, G.R., and Zimmerman, B.A. 1975, *Ann. Rev. Astr. Ap.*, *13*, 69.
Fuller, G.M., Fowler, W.A. and Newman, M. 1980, *Ap. J. Suppl.*, *42*, 447.
————. 1982, *Ap. J. Suppl.*, *48*, 279.
Habets, G.M.H.J. 1985, Ph.D. Thesis, University of Amsterdam.
————. 1986, *Astr. Ap.*, submitted.
Harris, M., Fowler, W.A., Caughlan, G.R., and Zimmerman, B.A. 1983, *Ann. Rev. Astr. Ap.*, *21*, 165.
Hashimoto, M., Hanawa, T., and Sugimoto, D. 1983, *Pub. Astr. Soc. Japan*, *35*, 1.
Hashimoto, M., and Nomoto, K. 1986, in preparation.
Hayashi, C., Hoshi, R., and Sugimoto, D. 1972, *Prog. Theoret. Phys. Suppl.*, *22*, 1.
Hillebrandt, W. 1986, this volume.
Hillebrandt, W., Nomoto, K., and Wolff, R.G. 1984, *Astr. Ap.*, *133*, 175.
Iben, I. Jr. 1986, this volume.
Ikeuchi, S., Nakazawa, K., Murai, T., Hoshi, R., and Hayashi, C. 1972, *Prog. Theoret. Phys.*, *48*. 1890.
Johnston, M.D., and Yahil, A. 1984, *Ap. J.*, *285*, 587.
Kahana, S.H. 1986, this volume.
Langer, N. 1986, *Astr. Ap.*, submitted.
Lattimer, J.M., Burrows, A., and Yahil, A 1985, *Ap. J.*, *288*, 644.
Lynden-Bell, D., and Wood, R. 1968, *M.N.R.A.S.*, *138*, 495.
Miyaji, S., Nomoto, K., Yokoi, K., and Sugimoto, D. 1980, *Pub. Astr. Soc. Japan*, *32*, 303
Miyaji, S., and Nomoto, K. 1986, *Ap. J.*, submitted.
Nomoto, K. 1981, in *IAU Symposium 93, Fundamental Problems in the Theory of Stellar Evolution*, ed. D. Sugimoto, D.Q. Lamb, and D.N. Schramm (Dordrecht: Reidel), p.295.
————. 1984a, *Ap. J.*, *277*, 791.
————. 1984b, in *Stellar Nucleosynthesis*, ed. C. Chiosi and A. Renzini (Dordrecht: Reidel), p. 238.
Nomoto, K. 1986, *Ann. N Y Acad. Sci.*, *470*, 294.
Nomoto, K., Thielemann, F.K., and Yokoi, K. 1984, *Ap. J.*, *286*, 644.
Saio, H., and Nomoto, K. 1985, *Astr. Ap.*, *150*, L21.
Schramm, D.N. 1986, this volume.
Sugimoto, D., Eriguchi, Y., and Hachisu, I. 1981, *Prog. Theoret. Phys. Suupl.*, *70*, 154.

Sugimoto, D., and Nomoto, K. 1980, *Space Sci. Rev.*, *25*, 155.
Thielemann, F.-K. 1986, private communication.
Thielemann, F.-K., and Arnett, W.D. 1985, *Ap. J.*, *295*, 604.
Weaver, T.A., and Woosley, S.E. 1980, *Ann. N Y Acad. Sci.*, *336*, 335.
Weaver, T A., Weosley, S.E., and Fuller, G.M. 1985, in *Numerical Astrophysics*, ed. J. Centrella, J. LeBlanc, and R. Bowers (Porola, CA: Science Book International), p.374.
Weaver, T.A., Zimmerman, G.B., and Woosley, S.E. 1978, *Ap. J.*, *225*, 1021.
Woosley, S.E., Fowler, W.A., Holmes, J.A., and Zimmerman, B.A. 1975, Caltech preprint OAP-422.
———, 1978, *Atomic Data and Nuclear Data Tables*, *22*, 371.
Woosley. S .E., and Weaver, T.A. 1986a, in *Nucleosynthesis and Its Implications for Nuclear and Particle Physics*, ed. J. Audouze and T. van Thuan (Dordrecht: Reidel).
———, 1986b, *Ann. Rev. Astr. Ap.*, in press.
Woosley, S.E., Weaver, T.A., and Taam, R.E. 1980, in *Type I Supernovae*, ed. J. C. Wheeler (Austin: University of Texas), p. 96.